ACS SyntheticBiology

Research Article

pubs.acs.org/synthbio

Biological Noise Abatement: Coordinating the Responses of Autonomous Bacteria in a Synthetic Biofilm to a Fluctuating Environment Using a Stochastic Bistable Switch

Edward M. Nelson,[†] Volker Kurz,[†] Nicolas Perry,[†] Douglas Kyrouac, and Gregory Timp*

Department of Biological Sciences and Electrical Engineering, University of Notre Dame, Notre Dame, Indiana 46556, United States

Supporting Information

ABSTRACT: Noise is inherent to single cell behavior. Its origins can be traced to the stochasticity associated with a few copies of genes and low concentrations of protein and ligands. We have studied the mechanisms by which the response of noisy elements can be entrained for biological signal processing. To elicit predictable biological function, we have engineered a gene environment that incorporates a gene regulatory network with the stringently controlled microenvironment found in a synthetic biofilm. The regulatory network leverages the positive feedback found in quorum-sensing regulatory components of the *lux* operon, which is used to coordinate cellular responses to environmental fluctuations. Accumulation of the Lux receptor in cells, resulting from autoregulation, confers a rapid response and enhanced sensitivity to the quorum-sensing molecule that is retained after cell division as epigenetic memory. The memory of the system channels stochastic noise into a coordinated response among quorum-sensing signal receivers in a synthetic biofilm in which the noise diminishes with repeated exposure to noisy transmitters on the input of a signaling cascade integrated into the same biofilm. Thus, gene expression in the receivers, which are autonomous and do not communicate with each other, is synchronized to fluctuations in the environment.

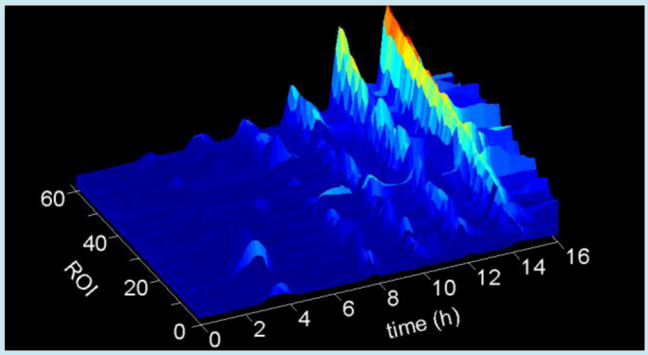

KEYWORDS: *synthetic biology, bistability, autoregulation, synthetic biofilm, stochastic noise, synchronization*

A biofilm is the archetypal biological smart material. It is a sessile yet complex multikingdom community of microorganisms. The complexity of a biofilm reflects environmental gradients in nutrients and flow conditions, and a variety of epigenetic and genetic constituencies that allow it to respond to changes in its environment no matter how inhospitable.[1−4] As a result of their metabolic versatility and phenotype plasticity, biofilms are found in everything from the interior of a pipe in a drinking water distribution system to acid mine drainage. Moreover, biofilms afford protection against environmental stresses such as oxidants, antibiotics, extreme pH shifts, or macrophages,[5] which is especially troublesome since they have been implicated in 60% of all infections.[4] Thus, the analysis of biofilm structure and function is motivated by health concerns, but it also informs on the design of tissue that is responsive to the environment as well as promoting a comprehensive understanding of individual cell function.

Bacteria within a biofilm can coordinate their response to an environmental stimulus through quorum-sensing (QS) signals.[6−10] According to the QS hypothesis, bacteria count their numbers by producing, releasing, and detecting small, diffusible, signaling molecules. QS coordinates differentiation in a biofilm, producing phenotype diversity that allows adaptation to the environment, has been implicated in bacterial surface motility[9] and biofilm architecture and may play a role in the exchange of genetic materials.[7,10] However, the information communicated by the QS signals can depend on the environmental conditions—the mixing, flow, density, distribution, and type of cells producing the signals and their antagonists.[11−14] This observation has prompted alternative views, which posit that the QS signal acts simply as a probe measuring mass transport in the microenvironment of an otherwise autonomous cell.[12,13]

Noise in the QS communication channel can compromise the coordination of the cellular response to environmental changes.[15−18] The origins of the noise can be traced to the stochasticity associated with a few copies of genes and low concentrations of protein and ligands either in the QS signal transmitter, the receiver or the medium connecting the two. It is shown here that noise in a signaling cascade can be suppressed by using stochastic, bistable switching elements found regularly in QS systems. To test for coordination in response to fluctuations in the environment and the effect of noise in the concomitant gene expression, *E. coli* were transformed with a (receiver) gene circuit component, the bidirectional promoter *luxP*, which has been associated with bistability in response to a QS signal, *N*-*β*-Ketocaproyl)-L-

Received: May 1, 2013
Published: October 3, 2013

homoserine lactone ($3OC_6HSL$ or AHL),[19,20] and then placed in a microenvironment that was strictly regulated. The left side of *luxP* (*luxP*(*L*)) controls LuxR production and the right (*luxP*(*R*)) controls production of a degradable variant of green fluorescent protein, GFP-LVA (see Figure S1(a,b) in the Supporting Information).[21] This gene component is derived from one of two interlocked feedback loops found in the *lux* QS circuitry of *V. fischeri*. The bistability is a hallmark of the positive autoregulation associated with this feedback loop, which modulates the expression of LuxR as part of the QS response. The bidirectional promoter *luxP* is bound by a LuxR-AHL dimer, strongly up-regulating expression of a transient fluorescent reporter, GFP-LVA, on the (R) side of the promoter and weakly upregulating expression of LuxR on the (L) side.

To produce predictable biologial function, (i.e., coordination) both the gene and its environment were stringently controlled by incorporating the transformed receiver cells into a synthetic biofilm using live-cell lithography.[22] Live-cell lithography ensured that each cell has unobstructed access to the environment, which was controlled through the microfluidic device, and that the response of cells could be easily tracked. Subsequently, a QS signal was broadcast simultaneously into the synthetic biofilm, and it was observed that noise in the cellular responses diminished with repeated exposure, indicating that gene expression becomes tightly coordinated. Stochastic simulations based on parameters that were all tightly constrained by known values in the literature were used successfully to predict experimental outcomes and revealed that the noise reduction was due to the memory inherent in the bistable element, which fades with each generation.

Cascading variable elements can also amplify noise.[15−17,23−25] Each step in a cascade receives a stochastic signal from its upstream transmitter and adds additional variability to it. To investigate the effect of a bistable switch on the noise in a communication channel, *E. coli* were transformed to act like a QS signal transmitter of AHL. These transmitters coexpressed degradable forms of LuxI (LuxI-LVA) and a GFP (GFP-LVA) reporter under a *lac* promoter upon induction with isopropyl-β-D-thiogalactopyranoside (IPTG). From normal metabolic products (*S*-adenosyl methionine and an acyl-ACP carrier protein used in fatty acid synthesis) the LuxI-LVA protein catalyzes production of AHL that then diffuses across the cell membrane out into the environment. Thus, AHL signal production is a stochastic process introducing concentration fluctuations in the environment of receivers placed nearby using live cell lithography. Interestingly, despite the noise in the transmitted signal, the receiver response is tightly coordinated after the initial pulse—the stochastic switch actually provides noise abatement—and the noise is suppressed compared to the transmitter.

In QS, there is no distinction between transmitting and receiving cells since each cell is both a transmitter and receiver.[6−9,26] In contrast, in this study, the *lux* QS circuitry was analyzed into two cell types, a transmitter and receiver, to test separately their noise performance and unambiguously determine the effect of the bistable switch. The transmitter can signal only a receiver—it cannot receive a signal—and the receiver transmits no signal at all. *Lux* (and *lac*) gene circuits were chosen to test coordination because many of the parameters that govern the reaction kinetics of the *lux* and *lac* operon are already known[27,28] making quantitative simulations of the experiments possible. Due to the small number of molecules involved, e.g., only 1−2 AHL molecules are needed to trigger the switch, stochastic simulations are required to faithfully capture the dynamics. Moreover, the bistable element is linked to a single protein, LuxR, so that the circuit components are supposed to interact primarily with each other and only minimally with the cell. This is important because even for simple networks that couple to the environment through intercellular signals, unwanted interactions of the designed network with other pathways can diminish control over biological function. To test for unwanted interactions, protein production was limited to LuxR and GFP-LVA via expression of an mRNA interferase, MazF.[29] When MazF interferase is overexpressed by external induction, it minimizes the production of most proteins in the cell by cleaving mRNA at ACA sequences, thereby forcing a quasi-quiescent state in the bacteria. Thus, the single protein production (SPP) strategy decouples LuxR production from other networks in the cell.

RESULTS AND DISCUSSION

It is hypothesized that the response of bacteria in a synthetic biofilm can be entrained to large fluctuations in the environment using a bistable element. To test this hypothesis, 203 and 203A plasmids were utilized (see Supplementary Figure S1a,b) consisting of a fragment of the *lux* network containing a bistable element found in the *lux* circuitry of *V. fischeri*, fused to a degradable variant of GFP gene. These plasmids contain a bidirectional promoter *luxP*: *luxP*(*L*) controls LuxR production, whereas *luxP*(*R*) controls the production of GFP-LVA.

It has been demonstrated elsewhere using RT-qPCR that in this system LuxR is constitutively expressed at a low level and is up-regulated 2-fold by AHL induction,[19] which is consistent with prior work that established bistabilty in this network.[20] However, bulk measurements like RT-qPCR can conceal variations in single-cell responses associated with bistability. Consequently, flow cytometry was used to reveal phenotypes in the population. Figure 1a shows scatter plots obtained from flow cytometry, illustrating three domains observed at 30 °C: two unimodal distributions found near 1 nM (LOW) and 10 nM (HIGH) concentrations of AHL and a third that is bimodal found near the bifurcation threshold at 2 nM. The bimodal distribution (Figure 1a), which is consistent with a bistable domain, has one fluorescent intensity peak comparable to the unimodal distribution at 1 nM and another with intensity that is 30-fold higher. As the AHL concentration increased beyond 2 nM, the populations coalesced into a unimodal distribution with a fluorescence intensity about 100-fold higher than that found at 1 nM.

To establish the parameters governing the luxR autoregulatory network, the Gillespie algorithm[30] was used, in conjunction with the model shown in Figure 1b, to simulate stochastically the cell fluorescence data. This model captures the kinetics of both LuxR and GFP-LVA in each cell (see Supplementary Tables S1, S2 and Figure S2). Figure 1c shows the number of fluorescent GFP molecules obtained from independent simulations of an ensemble of 10,000 cells induced by different concentrations of AHL for 2 h, in which each cell in the simulation was initialized with 50 LuxR molecules per cell (85 nM). The results indicate a bifurcation threshold for AHL concentrations between 1 and 2 molecules per cell (1.7−3.4 nM). For higher extracellular AHL concentrations, the cells

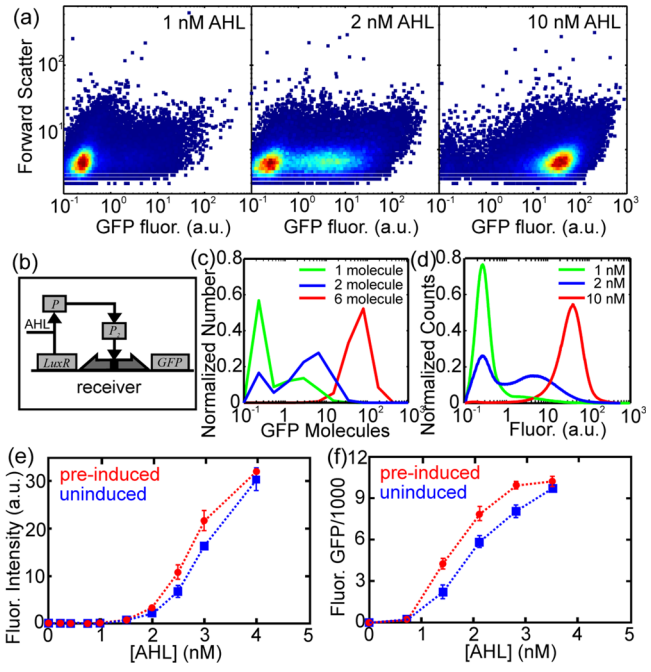

Figure 1. LuxR bistable switch characteristics. (a) Flow cytometry results showing the forward scattered versus fluorescence signal from 9 × 10^4 bacteria incorporating the 203A plasmid in 1, 2, and 10 nM concentration of AHL at 30 °C for 2 h demonstrating the bistability of the *lux* system. (b) Model of the QS receiver circuitry showing the operation of a LuxR-bistable switch used in stochastic simulation. The QS ligand, AHL, which is externally applied and is able to diffuse into and out of the cell, forms a complex with LuxR that enhances transcription of *GFP*-LVA. *P* represents the LuxR/*AHL* complex; P_2 is dimerized *P* that binds to the *lux* promoter, driving the expression of LuxR and GFP-LVA. (c) Single cell stochastic simulations of fluorescent GFP expression derived from the model in panel b. A histogram of levels obtained from an ensemble of 1 × 10^4 cells induced by 1, 2, and 6 molecules/cell (1.7, 3.4, and 10.2 nM) of AHL for 2 h. Details of the simulation are given in the text. (d) Histograms of the data shown in panel a for comparison to panel c. (e) The mean fluorescence of bacteria preinduced (red) with 100 nM of AHL or uninduced (blue) after a 10 h exposure to different concentrations of AHL. Error bars represent the fluorescent range from multiple (2) measurements. (f) Mean number of fluorescent GFP molecules in a simulated population of 100 bacteria that were initialized in either the HIGH state (preinduced, red) or in the LOW state (uninduced, blue) after a 10 h exposure to different concentrations of AHL. The error bars represent the standard deviation from multiple (10) simulations.

switch to the HIGH expression state based on the number of fluorescent GFP molecules in the system. Thus, according to the model, positive autoregulation produces bistability near 2 molecules of extracellular AHL per cell (3.4 nM). For comparison, Figure 1d shows a series of histograms of the fluorescence derived from the flow cytometry results shown in panel a. Likewise, for extracellular concentrations of AHL > 3 nM, the cells switch to the HIGH expression state based on the number of fluorescent GFP molecules in the system, indicating that positive autoregulation produces bistability at an AHL concentration of 3 nM.

Memory is a property of biochemical systems with bistability.[19,20] Under identical chemical conditions, the system can be in either one of two alternative states, HIGH or LOW, depending on its recent history. It is hypothesized that the memory in this system is held in the amount of LuxR in each cell. The amount of LuxR affects the sensitivity of the bacteria to AHL exposure: high levels of LuxR (HIGH state) allow the bacteria to respond to lower levels of AHL, whereas cells with low levels of LuxR (LOW state) are unresponsive without higher levels of AHL. Changes in the memory status can occur either through production of LuxR via induction with AHL (LOW → HIGH) or via dilution of the LuxR concentration over time through cell division (HIGH → LOW).

Assuming that the memory degrades only by cell proliferation, it was hypothesized that the luxR-autoregulation element integrates QS signals into an epigenetic memory that can persist for several generations. To confirm this hypothesis, the response of two cell populations to AHL was tracked over multiple generations with laser cytometry and stochastic simulations were used to interpret the data (Figure 1e,f). In these experiments, two clonal receiver populations were cultured for 12 h at 37 °C: one in 100 nM AHL (preinduced), well above the bifurcation threshold, to promote a population in the HIGH state and another without (uninduced). Subsequently, each culture was diluted (1:10,000) into fresh media and then used to seed several separate populations that were, in turn, dosed with various amounts of AHL near the bifurcation threshold. These populations were then cultured at 30 °C for 20 h (about 10 generations in liquid culture, where the doubling time is 120 min) and characterized by laser cytometry (Figure 1e).

The induction profile of the receivers was observed to depend on the history of the seed culture—the response was hysteretic indicating bistability and memory. In the range from 2 to 4 nM AHL, the population that originated in the HIGH expression state showed a higher fluorescence, or in other words, the preinduced cells sustained the HIGH state even after 10 generations in a low-level AHL environment, while the uninduced cells did not, responding as naive cells would. Likewise, simulations that followed the evolution of two populations containing 100 cells each reproduced this trend. As in the experiment, one population was forced to the HIGH expression state with 500 ± 50 LuxR molecules per cell (50 nM), whereas a second population was initialized in the LOW state with 50 ± 10 LuxR molecules per cell. Then each population was exposed to low concentrations of AHL for 10 simulation hours, and the resulting number of fluorescent GFP-LVA in each cell was counted (Figure 1f). The preinduced population showed increased fluorescence even after 10 generations relative to the uninduced population, supporting the interpretation that the bistability gives rise to an epigenetic memory held in the concentration of LuxR.

Noise develops in the cellular responses if the number of either AHL or LuxR molecules is too low. However, the memory held by LuxR can be used to coordinate gene expression by driving a cell at or above the bifurcation point. This is demonstrated by subjecting a superarray of bacteria to a fluctuating environment of AHL, while simultaneously measuring the corresponding changes in the fluorescence of individual receivers. A fluctuating environment is closer to the natural environment than a standard culture and so provides a useful framework in which to demonstrate coordination.[18]

The transmission image of a superarray at t = 0 h, just prior to induction by AHL, is shown in Figure 2a. After assembly, different concentrations of AHL are introduced at a rate of 3 μL/min for varying lengths of time. The diffusion coefficient of AHL in the hydrogel was estimated to be greater than $D^{\text{hydrogel}}_{\text{rhodamine}}$ = 17 ± 10 $\mu m^2/s$, using a fluorescent surrogate with a similar molecular weight (see Supporting Information and Supple-

dx.doi.org/10.1021/sb400052f | *ACS Synth. Biol.* 2014, 3, 286−297

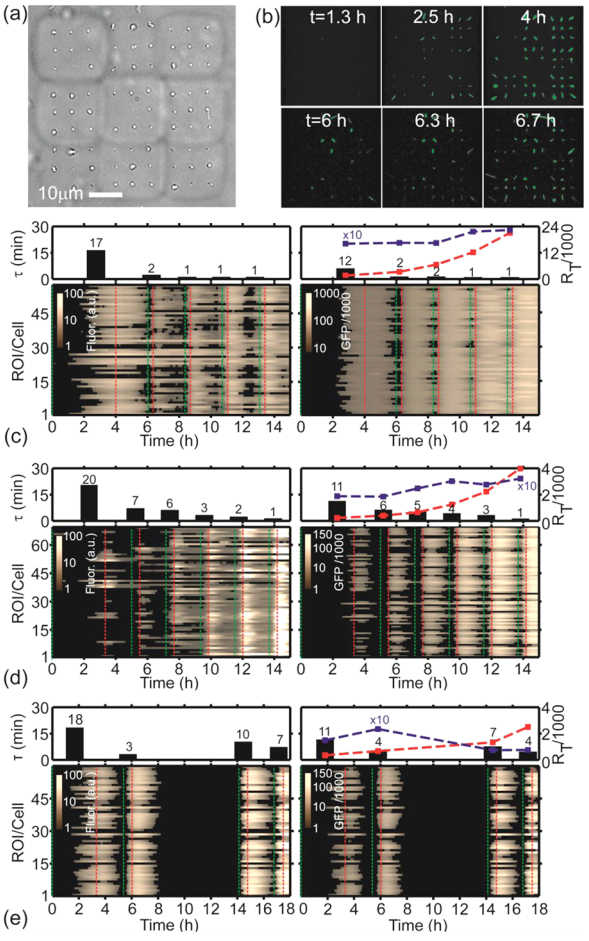

Figure 2. Entraining a superarray of 203 bacteria at saturating and near threshold concentrations of AHL. (a) Transmission image of a 3 × 3 superarray of homologous 3 × 3 microarrays of 203 bacteria (81 cells) in a microfluidic at $t = 0$. (b) Fluorescence images of the same array at times corresponding to the first ($0 < t < 4$ h) and second ($6.0 < t < 6.3$ h) 100 nM AHL pulse in M9 media. The fluorescent response between 1.3 and 4 h shows asynchronous behavior; the onset of the fluorescence is distributed over 160 min, whereas the onset of the fluorescence between 6 and 6.7 h is coordinated within 20 min. (c) (Left) A kymograph of the time evolution of the logarithm of the fluorescent intensity of 57 ROIs in the superarray shown in panel a. 100 nM AHL was introduced at $t = 0$ h, ending 4 h later, and subsequently at $t = 6$, 8.3, 10.7, and 13.0 h, each lasting 0.5 h. The beginning and end of each AHL broadcast are represented by green and red lines respectively. The mean lag τ between the signals is shown in the bar graph above the kymograph. (Right) Stochastic simulation of the production of fluorescent GFP in conditions identical to the experiment represent in panel c, left, initialized with 50 ± 10 LuxR molecules per cell (85 ± 17 nM) and 10 DNA operators per cell. The bar graph above the kymograph summarizes the corresponding τ of the simulation and the total number of R molecules in a microcolony (red) or single cell (blue). (d) (Left) similar to panel c, but introducing only 5 nM AHL pulses starting at $t = 0$ h and ending at 3.5 h and starting again at $t = 5.5$ h and ending 0.5 h later, etc. (Right) Stochastic simulation of the production of GFP-LVA protein in conditions identical to the experiment represent in panel d, left. (e) (Left) Similar to panel d in which two 5 nM AHL pulses are introduced initially, but with a multigeneration time lapse (8 h) before the next set of pulses to show the effect of a deteriorating epigenetic memory. The beginning and end of each AHL broadcast are represented by green and red lines respectively. (Right) Stochastic simulation of the production of GFP-LVA protein in conditions identical to the experiment represent in panel e, left.

mentary Figure S3d), which is less than 5% of the value measured for free diffusion of the same ligand in water ($D^{\text{water}}_{\text{rhodamine}} = 424\ \mu m^2/s$), but consistent with a high cross-linking density in the PEGDA.[31,32] As a result, after broadcasting the AHL into the superarray from the microfluidic device, the concentration is estimated to be practically uniform, varying <1% throughout the array within 90 s (Supplementary Figure S3). Between cycles, AHL is flushed from the environment by flowing minimal media at 60 μL/min for 8 min.

Figure 2b contrasts the fluorescence obtained from such an array during the first and second 100 nM AHL pulses, respectively. The first 100 nM AHL pulse is broadcast into the array at $t = 0$ h, but the onset of fluorescence is not detected until $t = 1.3$ h. Part of the delay between the start of the pulse and the fluorescence is attributable to the time required by the cell to exit the shock state associated with the assembly process.[11] The delay as well as the strength of the fluorescence depends on the idiosyncrasies of the cells comprising the array as well. For example, the plasmid copy number, the metabolic level of individual cells, asynchrony of the cell cycle, and the fluctuating reactivity of biologically relevant molecules in each cell can all give rise to random variations in the fluorescence response time. Among the regions-of-interest (ROI) selected here, the range between the first and last cell's detectable fluorescent response is ∼2.7 h.

At $t = 4$ h, the AHL concentration is reduced to zero and the fluorescence decays to the background on a time scale (45 min) consistent with proteolytic digestion associated with the LVA tag. Subsequently, a second pulse is broadcast into the superarray at $t = 6$ h, while the fluorescence is continuously monitored. (The 2-h-long cycle without the AHL inducer ensures that there is no residual fluorescence measured in a subsequent induction cycle.) Interestingly, it is observed that the delay before the onset of fluorescence is now only ∼0.33 h (Figure 2b). After 0.5 h of induction, the AHL concentration is flushed to zero, and the cycle is repeated again at $t = 8.3$, 10.7, and 13.0 h with similar results; the onset of fluorescence for each of the ROIs occurs within 20 min of each other in stark contrast with the results following the initial exposure.

The kymograph, Figure 2c, left, tracks the logarithm of the fluorescence of each ROI in the array, illustrating the asynchronous timing of the response to the first AHL pulse and the entrainment to each pulse thereafter. (The same data is exhibited in multiple line plots on a linear scale in Supplementary Figure S4 and shows that the fluorescence was not allowed to saturate the detector.) Each ROI was defined to be 5 μm on edge so that initially it encompassed the length and breadth of a single bacterium in the synthetic biofilm. However, as the measured doubling time in the film was 185 ± 10 min, cell proliferation eventually led to multiple bacteria within each ROI. Still it is possible to follow the dynamics associated with a single cell with confocal microscopy, and a comparison shows that the same trends are observed with a 5 μm ROI (see Supplementary Figure S5). Thus, the scope of a ROI 5 μm on edge was used to define the volume of the stochastic response.

To quantify the coordination of responses between ROIs, we introduced the similarity function:[33]

dx.doi.org/10.1021/sb400052f | ACS Synth. Biol. 2014, 3, 286−297

$$S_{ij}(\Delta t) = \sqrt{\frac{\langle [x_i(t+\Delta t) - x_j(t)]^2 \rangle}{[\langle x_i^2(t)\rangle \langle x_j^2(t)\rangle]^{1/2}}} \text{ with } \tau \equiv |\Delta t|_{S_{ij}=\min}| \quad (1)$$

Here, $x_i(t)$ is a measure of the fluorescence of cell i at time t, and Δt is the time differential between the signal responses. For our purposes, the logarithmic derivative of the fluorescence was used as a measure of the fluoresence to improve sensitivity to weak signals (see Materials and Methods). The gauge of coordination between different cells, τ, is defined as the absolute value of the differential Δt that minimizes S. In other words, τ is the offset required to superimpose the two responses. Ideally, a system in perfect coordination would display no time shift or $\tau = 0$. On the other hand, if cells express GFP at different times in relation to external stimuli (i.e., $\tau \neq 0$), then the system is uncoordinated with that stimuli. For the five 100 nM AHL pulses broadcast into the array in Figure 2c, the mean differential among all the ROIs is τ_0 =17 min for the first pulse but improves to τ = 1 min after the second pulse as shown in the bar graph above the kymograph. Therefore, while the system response is initially uncoordinated, the cells quickly become entrained to the environment after the first pulse.

In contrast with the data obtained at high AHL concentration, the coordination between the cellular responses develops more gradually with time for concentrations near the bifurcation threshold. The kymograph in Figure 2d, left, illustrates the development of the logarithm of the fluorescence for a similar superarray, exposed to 5 nM AHL pulses only, a concentration closer to the bifurcation threshold. The first AHL pulse is broadcast into the array at t = 0 h, but the onset of fluorescence is not observed until 2 h later. At t = 3.3 h, the AHL concentration is reduced to zero, and after 0.5 h of induction the cycle is repeated: flushing the AHL concentration back to zero, and broadcasting 5 nM of AHL again at t = 5, 7.2, 9.3, 11.5, and 13.7 h for 0.5 h each. For the six 5 nM AHL pulses broadcast into the array, it was found that τ_0 = 20, τ_1 = 7, τ_2 = 6, τ_3 = 3, τ_4 = 2 min, and finally τ_5 = 1 min after 13.7 h as delineated by the corresponding bar graph. Altogether, more than 26 experiments like those exhibited in Figure 2 were performed but with different concentrations and cycling. All of them followed the same trend in which coordination led to shorter time differentials in the response with increased cycles. Therefore, this trend in the time differential cannot result from the quantitative differences of the cycle waveforms.

To track the persistence of the memory, another superarray was exposed to similar conditions as the experiment in Figure 2d, but with an intervening lapse. The kymograph in Figure 2e, left, shows the development of the logarithm of the fluorescence, whereas the corresponding bar graph quantifies the coordination. The first AHL pulse is broadcast into the array at t = 0 h, and fluorescence is observed about 2 h later. At t = 3.5 h, the AHL concentration is flushed to zero, and after 2 h of induction, the cycle is repeated: a second 5 nM of AHL was broadcast at t = 5.5 h, which is then flushed to zero after 0.67 h. Subsequently, no AHL flows through the superarray until t = 14 h, at which time 5 nM of AHL is broadcast into the array for 0.67 h and then flushed, and then once again at t = 16.7 h 5 nM of AHL is broadcast into the array. The uncoordinated responses to the first 5 nM pulse, measured by τ_0 = 18, became more synchronized after a second 5 nM exposure since τ_1 = 3, but after the intervening 8 h lapse (2.6 generations) in exposure to AHL, a third 5 nM pulse shows evidence of deterioration in the coordination since τ_2 = 10. During the lapse, the cells proliferate, and it is assumed that the memory held in LuxR fades by dilution. However, improvement in the coordination is still possible as another 5 nM pulse after that produces τ_3 = 7. Thus, the epigenetic memory of contact with an AHL concentration above the bifurcation threshold fades after 2−3 generations without exposure but recovers with recurring contact.

Stochastic simulations of GFP-LVA production under conditions identical to the experiments in Figure 2c−e were performed to unravel the relationship between cell coordination, LuxR, and AHL. The simulations followed the time evolution of the external AHL concentration quantitatively and were tightly constrained by parameters known from the literature.[27] The simulation results are summarized in the kymographs shown on the right-hand side of Figure 2c−e, which faithfully captured the essential aspects of the experiment, i.e., the same rate of growth and decay of GFP-LVA on average as observed in the experiment. For 100 nM AHL, the mean number of LuxR in each cell (blue dashed lines) exceeds 1500 molecules after the first pulse, which gives rise to a persistent memory. On the other hand, for 5 nM AHL pulses, the mean number of LuxR molecules in each cell does not surpass 200 until after the second pulse, leading to a delay in the coordination of the communal response. Evidently, the low level of ligand lowers the probability of the system to go from the LOW to the HIGH state. Finally, whereas the number of LuxR in each cell exceeds 200 molecules per cell after the second 5 nM pulse in the experiment of Figure 2e, that number diminishes with cell proliferation to <100 LuxR after 8 h, with the concomitant loss of memory causing a corresponding degradation in coordination.

To establish how the number of LuxR molecules affects synchronization, an ensemble of 100 cells with high-copy plasmids, induced for 2 h, was simulated with different AHL concentrations. The results shown in Figure 3a indicate that there is a significant improvement in the similarity (open symbols) between different cells as the concentration of AHL increases. For concentrations above 4 molecules (6.8 nM) of AHL per cell, the cells are highly synchronized (τ < 5 min) regardless of the amount of initial LuxR in each of the cells. Also, the similarity between cells is inversely correlated to the total number of LuxR molecules as indicated by the mean number of LuxR after 2 h (solid symbols). When the number of LuxR becomes greater than 500 molecules per cell (0.85 μM), coordination improves to τ < 5 min, which is consistent with the simulation results shown in Figure 2. Cells that begin with a low number of LuxR molecules (squares) take longer than 2 h to synthesize the necessary amount of LuxR for entrainment and have low ensemble similarity. On the other hand, the cells with a high initial number of LuxR molecules (circles) can quickly respond to the environment, even when the number of external AHL is below the threshold for bistability, indicating that the amount of LuxR in each of the cells determines the response to the environment. Only when LuxR exceeds about 500 molecules per cell (0.85 μM) is the response well coordinated. From this inference, it is concluded that it is the total number of LuxR molecules that affects coordination in the communal response.

Accordingly, a deterministic sensitivity analysis was performed on the model to resolve the relationship between the different kinetic parameters and LuxR. The sensitivity of a dynamic system is a measure of the degree to which one species

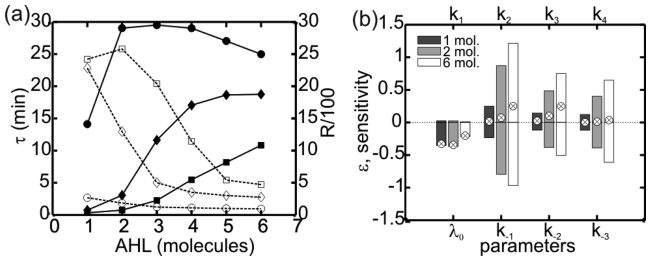

Figure 3. Sensitivity analysis of a stochastic LuxR bistable element. (a) Measure of coordination, τ, calculated from the stochastic simulation of a 100-cell ensemble that was induced for 2 h by different concentration of external AHL (dotted line). Each simulation was initialized with either 50 (squares), 100 (diamonds), or 500 (circles) LuxR molecules per cell (85, 170, 850 nM). The mean number of R molecules at the end of 2 h for each concentration is represented by filled symbols. The lines are guides to the eye. (b) Elasticity (ε) of R to various kinetic rate pairs after 2 h for 1, 2, or 6 molecules (1.7, 3.4, or 10.2 nM) of external A. The forward and reverse rate parameters are grouped together according to equations S(i–iv) in the Supporting Information. Here, k_0 is LuxR basal production; k_1 is the association rate between R and A; k_2 is the dimerization rate of P; k_3 is the binding rate between P_2 and operator (O_R); λ_0 is degradation rate of LuxR; k_{-1} is the dissociation rate of P; k_{-2} is the dissociation of P_2; and k_{-3} is the dissociation rate of the P_2O_R complex. The net rate sensitivity of each reaction pair is indicated by the symbols. Below the threshold for bistability (1 molecule of A or 1.7 nM) the rate parameters have either a negative or neutral effect on R states. Above the threshold for bistability binding between R and A, and dimerization of P contributes the strongest to the R state.

is affected by different parameters. For example, the time-dependent sensitivity, also known as the *elasticity*, between state v and the parameter p is given by $\varepsilon = \partial v(t)/\partial p$.[34] The elasticity of LuxR to various kinetic rates after 2 h for different amounts of external AHL is shown in Figure 3b. For this simulation, the cells were initialized with 50 ± 10 LuxR molecules per cell (85 ± 17 nM). For simplicity, the forward and reverse rate parameters are grouped together according to the rate equations S(i–iv) in the Supporting Information. The combined rate sensitivity (symbols) indicates that below the threshold for bistability (2 molecules/cell or about 3 nM of external AHL) the net effect of each reaction is either negative (suppresses LuxR production) or neutral (no effect on production). Above the AHL threshold, the formation of the complex *P*, as well as the subsequent dimerization of *P*, has the largest effect on the amount of LuxR. Thus, the production of LuxR, and by extension the development of memory and enhanced response to AHL, is most sensitive to the forward rates, k_1, k_2, and the reverse reaction rates k_{-1}, k_{-2}.

The results obtained from two separate control experiments offer further support for the interpretation that the Lux receptor in cells resulting from autoregulation exclusively channels stochastic noise into a coordinated response in the receiver. The first control tests for coordination in the absence of the *lux* circuitry, whereas the second tests for coordination in the absence of a bistable switch. First, to determine if the system memory is attributable to the *lux* circuitry exclusively, a plasmid (M2) was constructed from a hybrid of *trp* and *lac* promoters called *tac*,[35–37] replacing *lux* as the regulator of GFP-LVA expression (see Supplementary Figure S1c). Pulses of 500 μM IPTG in M9 media lasting 1.5 h followed by 3-h-long pulses of media were used to induce the cells; the resulting fluorescence is summarized in the kymograph shown in Figure 4a. It is apparent from the persistently high value of τ that the fluorescence is uncoordinated compared to the data of Figure

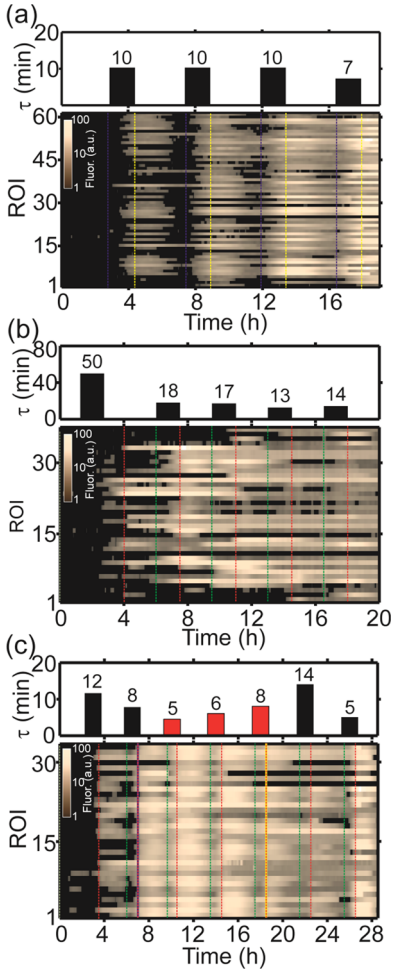

Figure 4. Control response of three superarrays incorporating different sensing circuitry to a fluctuating environment. (a) Kymograph showing the evolution of the log fluorescence intensity observed in M2 (lac regulated cells) with 1.5 h pulses of 500 μM IPTG. The beginning and end of each IPTG broadcast are represented by blue and yellow lines, respectively. The coordination of GFP-LVA expression in M2 does not improve substantially with time but remains consistent as shown in the τ bar graph. (b) Kymograph showing the evolution of the log fluorescence intensity observed in M3 (constitutively expressed LuxR under control of a *araB* promoter) with 1.5 h pulses of 1 μM AHL without arabinose, similar to Figure 2c. The expression of LuxR is controlled by a leaky *araB* promoter so that in the absence of arabinose the gene circuit produces sufficient LuxR to observe a response to AHL. The beginning and end of each AHL broadcast are represented by green and red lines, respectively. The coordination of GFP-LVA expression in M3 does not improve substantially with time but remains consistent as shown in the τ bar graph. (c) Coordination of GFP-LVA fluorescence in 203A+MazF (SPP) cells. The kymograph shows the evolution of log fluorescence intensity while the cells are induced by 60-min-long pulses of 500 nM AHL followed by 180-min-long pulses of M9 media without AHL. The beginning and end of each IPTG broadcast are represented by blue and yellow lines, respectively, whereas the beginning and end of each AHL broadcast are represented by green and red lines, respectively. After the first two cycles, starting at t = 7 h, 100 μM IPTG is added to induce MazF expression, shutting down protein production except for LuxR and GFP-LVA until t = 18.5 h. The resulting bar graph measures the change in synchronization with MazF.

dx.doi.org/10.1021/sb400052f | *ACS Synth. Biol.* 2014, 3, 286–297

2c. Thus, the lack of coordination observed initially is not associated with variations in initial concentration of LuxR alone, nor is the subsequent entrainment exhibited in Figure 2c attributable to GFP-LVA production. Rather, the coordination is due to some specific aspect of the *lux* system, presumably the autoregulation of LuxR concentration.

Second, to establish that the noise suppression is attributable to the autoregulation of LuxR exclusively, the plasmid M3 was constructed by placing strong transcriptional terminators downstream of the *luxP*(*L*) promoter in the bidirectional switch and placing LuxR under control of an *araB* promoter instead (Supplementary Figure S1e). Accordingly, LuxR is constitutively expressed when arabinose is found in the environment, although the promoter is leaky enough to produce sufficient LuxR to observe some sensitivity to AHL even in the absence of arabinose. For comparison to 203 receivers, an M3 superarray was induced with 2 μM AHL for 4 h followed by a 2-h flush with media without AHL. Subsequently, pulses of media with 2 μM AHL were broadcast into the array for 1.5 h at 6, 9.5, 13.0, and 16.5 h. The measured fluorescence (Figure 4b) shows a persistent and high value of τ (τ_0 = 50 min, τ_1 = 18 min, τ_2 = 17 min, τ_3 = 13 min, and τ_4 = 14 min) in the M3 array, indicating an uncoordinated response compared to the data of Figure 2c. (The initial τ-value of 50 min is mainly due to the lack of a response within the first induction cycle since only 4 cells are responding). Thus, the noise suppression observed in Figure 2c after the first pulse is unambiguously associated with the bidirectional promoter *luxP*, which is linked to a single protein, LuxR.

Whereas it is anticipated that this Lux autoregulatory circuit interacts only minimally with the cell, simple networks with coupling to the environment can produce unwanted interactions of the designed network leading to diminished control over biological function. To discover if the observed coordination is coupled to other cellular processes, SPP was used to isolate the *lux* circuitry from the cell metabolism. The SPP strategy forces the cell into a quasi-quiescent state that is evident in the comparison of the growth curves for 203 and 203A shown in the Supplementary Figure S6, which decouples ACA-less LuxR and GFP-LVA production from other networks in the cell.[29] To exaggerate the effect, we used a high-copy 203A plasmid along with MazF under control of *lac* (see Supplementary Figure S1d).

During this experiment, the cells were repeatedly induced with 1-h-long cycles of 500 nM AHL in media followed by a 3 h flush without AHL. However, after the end of the second cycle and until the end of the fifth cycle, 100 μM IPTG was broadcast into the superarray to affect the cell metabolism by inducing MazF. The results are summarized in Figure 4c. The corresponding τ-bar graph reveals that the 203A coordination improved initially from τ_0 = 12 to τ_1 = 8 min and continued to improve shortly after induction of MazF to τ_2 = 5 min but eventually became uncoordinated to τ = 14 min as the cells entered quasi-quiescence. While the approach to a coordinated communal response was not as rapid as initially observed for the 203 strain at 100 nM AHL, it was nevertheless consistent with the time-scale exhibited by 203A without MazF, as indicated in the Supplementary Figure S7. Only after the IPTG broadcast terminated and the cell eventually exited from the shock of MazF induction did the coordination recover to τ_6 = 5 min. Thus, the data supports the contention that the *luxR* circuitry can be used to coordinate protein production among the cells, but the cell's response is apparently inextricably linked to its metabolism as well.

Finally, to test the effect of a bistable switch in the receiver on the overall noise that develops in a signaling cascade, we transformed *E. coli* to act like QS signal transmitters (113) (see Supplementary Figure S1f), expressing degradable forms of LuxI (LuxI-LVA) and a GFP (GFP-LVA) reporter under a *lac* promoter. The expression of LuxI-LVA in the 113 transmitter facilitates the synthesis of AHL transiently by leveraging the cells metabolism until it degrades. Subsequently, the AHL diffuses into the environment and reaches the 203 receivers, which triggers the bistable switch in the receivers producing GFP-LVA and LuxR. Figure 5a shows a typical superarray consisting of transmitter and receiver cells; the transmitters are highlighted in red and the receivers in green. The model for transmitters is placed alongside that of the receivers in Figure 5b for comparison.

The kymograph in Figure 5c shows the time development of the logarithm of the fluorescence of each transmitter ROI, illustrating the asynchronous timing observed associated with the first three 0.75 mM IPTG pulses broadcast into the transmitter array. (The same data is shown in line plots of the fluorescence versus time plot in Supplementary Figure S8a.) The first IPTG pulse is broadcast into the array at t = 0, but the onset of fluorescence is not observed until 2 h later. Then at t = 5 h, the IPTG concentration is reduced to zero for 2 h. Starting at t = 7 h, the IPTG induction cycle is repeated twice more: broadcasting IPTG for 2 h, flushing to zero for 2 h, and then broadcasting IPTG again at 11 h for 2 h. Corresponding to the three IPTG pulses broadcast into the array, the mean time differential among all of the cells is τ_0 =15 min for the first pulse, whereas τ_1 = 5 and τ_2 = 6 min for the subsequent two pulses, respectively, as shown in the bar graph above the kymograph. Therefore, the transmitter cells, which are initially uncoordinated, become only weakly entrained to the IPTG in the environment.

On the other hand, Figure 5d illustrates the tightly coordinated response of the receivers in the same superarray after the initial pulse from the transmitters. The relatively noisy transmitters conveying AHL into the superarray initially produce an uncoordinated response among the receivers measured by the time differential τ_0 = 41 min, corresponding to the first IPTG pulse. However, after the second and third broadcasts of IPTG, the time differential falls below 3 min to τ_1 = 1 and τ_2 = 2 min, respectively. Thus, the noise in the receiver circuit is substantially reduced after the initial pulse measured relative to the noise in the transmitters in the same array.

To investigate the interrelationships between the number of LacI, LuxI-LVA, GFP-LVA, and AHL molecules produced in the transmitters and the LuxR and GFP-LVA produced in the receivers, the dynamics were simulated under the conditions of the experiments described in Figure 5c,d. The simulation results, which are summarized by corresponding kymographs in Figure 5c, right, and d, right, for the transmitters and receivers, respectively, capture the entrainment observed in the experiment. In particular, except for the first pulse, the bar graphs above each kymograph agree quantitatively with the time differentials measured in the transmitter and receivers. We attribute the difference between simulation and experiment in the first pulse to very weak fluorescence and instrumental noise there and other sources of stochastic variations that are not included in the model.

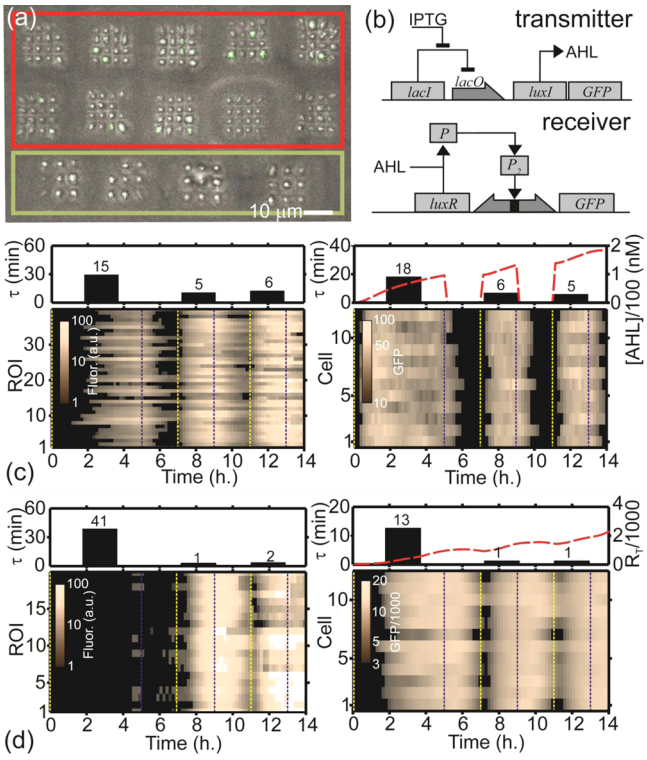

Figure 5. Coordinated response of a 203-receiver array to a noisy array of 113 transmitters. (a) Transmission image of a 2 × 5 superarray of homologous 4 × 4 microarrays of 113 transmitter bacteria (160 cells) highlighted in red, alongside a 1 × 4 superarray of homologous 3 × 3 microarrays of 203 receiver bacteria highlighted in green in a microfluidic at t = 0. (b) Model of the transmitter and receiver circuits. (c) (Left) Kymograph of the time evolution of the logarithm of the fluorescent intensity of 40 ROIs in the transmitter (113) portion of the superarray shown in panael a. A concentration of 0.75 mM of IPTG was broadcast into the array at t = 0 h, ending 5 h later; and subsequently at t = 7 and 11 h, each lasting 2 h. The beginning and end of each IPTG broadcast are represented by blue and yellow lines, respectively. The mean time differential between the signals, τ, is shown in the bar graph above the kymograph. (Right) Stochastic simulation of the production of fluorescent GFP-LVA in 12 cells under conditions identical to the experiment represent in panel c, left, with an initial 40 LacI molecules/cell (68 nM) and 10 DNA operators/cell. The bar graph above the kymograph summarizes the corresponding τ and AHL concentration at the receivers, inferred from the simulation. (d) (Left) Kymograph of the time evolution of the logarithm of the fluorescent intensity of 20 ROIs in the receiver 203 portion of the superarray shown in panel a. The beginning and end of each IPTG broadcast are represented by blue and yellow lines, respectively. (Right) Stochastic simulation of the production of fluorescent GFP-LVA in 12 cells under conditions identical to the experiment represent in panel d, left, with an initial 50 LuxR molecules/cell (85 nM) and 10 DNA operators/cell. The bar graph above the kymograph summarizes the corresponding τ and the number of LuxR molecules inferred from the simulation.

From the correspondence observed after the first pulse, it is inferred that there are ∼40 LacI molecules (68 nM) in each transmitter, while the number of LuxR molecules in the receivers exceeds the critical value of 500 just after the first IPTG cycle ends, as evident from the plot in Figure 5d, at which time the concentration of AHL in the receiver array (located 25 μm from the transmitters) exceeds 95 nM. (By the end of the second cycle, the concentration exceeds 130 nM AHL.) Since the concentration of IPTG is >4.4 × 10^5 molecules/cell (0.75 mM), while the number LacI that is expressed constitutively is only ∼40 molecules/cell (68 nM), the number of LacI molecules (and the plasmid copy number) are critical factors limiting entrainment of the transmitter to $\tau \approx$ 5 min. The sensitivity analysis offered in the Supporting Information (see Figure S8c) lends further support to this hypothesis indicating that the constitutive expression and degradation of LacI molecules are the key factors affecting GFP production limiting coordination of the transmitter. On the other hand, with the transmitters exuding an AHL concentration in excess of the bifurcation threshold, the memory held in LuxR is established after the first IPTG pulse so that the time differential in the receiver array collapses to $\tau \approx$ 2 min and the response becomes tightly coordinated.

Discussion. We have created a simple artificial biofilm.[38] This simple model is used to explore the behavior associated with a stochastic bistable switch, *luxP*, like that found naturally in the QS circuitry of *V. fischeri*. The autoregulation of LuxR increases the level of receptor protein in response to the ligand, achieving a bistable effect like that observed in the expression of the lac operon in *E. coli*. The autoregulation of the LuxR also provides a memory for the system, increasing the sensitivity and removing variability via accumulation of the receptor protein. Using a sensitivity analysis, it was determined that for low initial receptor concentration, the time scale for receptor−ligand binding was the limiting factor in cell activation. By increasing the receptor concentration so that it was no longer the rate-limiting step, different cells' responses to an externally applied ligand were coordinated. Similar behavior has been previously reported.[41,42] In the *lac* operon,[41] it was attributed to a positive feedback loop driving LacY, a transport protein that acts to concentrate *lac* inducer in the cell. Using an SPP system, the cells were restricted to the production of only GFP-LVA and LuxR. In this case, the system seems uncoordinated, presumably due to a combination of metabolic effects and autoregulation of the *lux* receptor indicating that the metabolism is inextricably linked to the biological function. Nevertheless, stochastic simulations based on a simple model of the switch accurately account for the observed behavior.

It is evident from the data of Figures 2 and 5 that the communal behavior in the receivers, which are not communicating with each other, can produce a tightly coordinated response that is synchronized to fluctuations in the environment arising either from broadcasts originating exogenously either from the microfluidic or from transmitters without the need for the entire QS machinery—only the bistable switch is required. Thus, even though the receivers do not communicate with each other and are autonomous, nevertheless their response is apparently synchronized. While it was demonstrated recently that bacteria can be mutually synchronized using a clock implemented in a gene circuit incorporating QS,[43,44] there are several shortcomings to this scheme for synchronization to the environment as mentioned earlier.[18] In contrast, stochastic bistable switches like those found in QS systems belong to another class of nonlinear systems that may be better suited to the task of synchronization.[16,18,45] Moreover, the coordination of the response between the elements of a biological system that each contain a bistable switch may come with a minimal metabolic load associated with the production of a single protein.

Using live cell lithography, this model can be generalized easily to mimic natural architectures that contain open water channels and a heterogeneous multikingdom consortium of

dx.doi.org/10.1021/sb400052f | ACS Synth. Biol. 2014, 3, 286−297

microorganisms.[22,39,40] Bacteria in native biofilms are exposed to a variety of environmental signals, e.g., cells near the center of a microcolony may experience low oxygen tension or high pH. Gradients can also be created in a hydrogel structure using a multiport microfluidic device.[19] Furthermore, signals such as common metabolites[46] or even antibiotics[47] possess many of the characteristic features of QS signals. In particular, methanogens, which are fastidious anaerobes not easily bent to experimental manipulation in the laboratory due to their complex nutritional requirements that cannot be satisfied in a monoculture, are of practical interest for an energy-starved world. Synthetic biofilms offer a platform for culturing methanogens by incorporating the correct populations of syntrophs to satisfy their nutritional requirements, and the analysis of QS signaling offers insight into nutrient exchange. Thus, it should be possible to use models like these, in which both the gene and its environment are stringently controlled, to create smart materials in which different strains or species are wired together to deliver complex, predictable biological functions.

Conclusion. To elicit a predictable biological function, i.e. coordination of protein expression, a gene environment was created using live cell lithography to form a synthetic biofilm from bacteria transformed with autoregulatory components in the *lux* QS system. Initially, protein production in the cells comprising the biofilm, measured by the fluorescent response of a reporter, was asynchronous. However, after subsequent pulses of a QS ligand, either supplied exogenously through a microfluidic device or from genetically engineered transmitters embedded in the film, the cell's response to fluctuations in the environment became tightly coordinated. In particular, the noise in the receiver was diminished relative to a noisy transmitter. The coordination was attributed to an adapted sensitivity associated with positive autoregulation of the Lux receptor. The correspondence with stochastic simulations, accomplished with tightly constrained parameters known from the literature,[27] not only supports these conclusions but also indicates that the function is predictable, despite the stochastic nature of the switch and coupling to the cell metabolism.

MATERIALS AND METHODS

Strains, Plasmids, and Genes. *E. coli* (DH5α) was transformed with various plasmids to produce QS signal transmitters (113) and receivers (203 and 203A); see Supplementary Figure S1. Like 203, 203A responds to AHL, but it contains coding sequences for LuxR and GFP-LVA that are devoid of ACA sequences as part of an SPP system. To construct an SPP system, ACA-less variants of the LuxR and GFP-LVA genes coding sequences were prepared by chemical synthesis (Genescript, Piscataway, NJ) following Suzuki et al.[29] Specifically, we synthesized a 203A plasmid with every ACA sequence in LuxR and GFP-LVA substituted for a synonymous triplet in such a way that mRNA translation was unchanged. We then cotransformed *E. coli* with both the 203A and pMazF. pMazF switches the cell to a SPP system upon induction by IPTG.

Two other plasmids were constructed to be used as controls for response of 203 to external inducer: M2 and M3 (Supplementary Figure S1). Plasmid M2 contains a GFP-LVA gene under the control of the *tac* promoter, which is induced by IPTG, while lacI is under control of a LacIq (constitutive) promoter, thus assuring that the inducer would not affect the expression of the transcription factor (lacI) (unlike the autoactivation loop of LuxR in 203.) Plasmid M3 was designed to eliminate the autoactivation loop, which was accomplished by modifying 203 such that the LuxP (L) promoter was blocked, and the LuxR gene was driven by the *AraB* promoter.

The bacteria were grown in M9 (0.2% glycerol) minimal media supplemented with 200 μM thiamine and 0.2% (w/v) casamino acids, using either kanamycin (50 μg/mL), ampicillin (100 μg/mL), or chloramphenicol (34 μg/mL) as selection markers. Cultures were incubated at 37 °C overnight, diluted 1:10 in fresh media, and harvested when they reached an optical density (OD_{600}) of 0.6−0.7.

Microfluidic Device. A microfluidic device was formed from polydimethylsiloxane (PDMS, Sylgard 184, Dow Corning) using a mold-casting technique; the channel was 600 μm tall, 1 mm wide, and 10 mm long. The master mold (FineLine Prototyping) is made of DSM Somos ProtoTherm 12120. To provide optical access we sealed the bottom of the PDMS microfluidic to a no. 1 cover glass using an oxygen plasma (PDS-32G, Harrick Plasma).[11,22] Finally, the microfluidic channels were connected to external syringe pumps through Tygon tubing.

Live Cell Lithography. A microfluidic channel was used to convey the genetically engineered bacteria to an assembly area where they were organized into superarrays of genetically engineered *E. coli* using optical tweezers as described elsewhere.[22] Optical trapping was accomplished in the center of the microfluidic in near static flow conditions. Bacteria were captured individually and placed into a time-shared array of optical traps using a freely definable "shepherd" beam; time-averaged powers in the array and shepherd beam were <1 mW and ∼3mW, respectively. Assembly of each microarray required <1 min. Each superarray comprised several regular 2D 3 × 3 microarrays as illustrated in Figure 2a. Adjacent microarrays were spaced 22 μm apart (in *X* and/or *Y*), using a motorized *X*-*Y* stage (MS2000) with 0.25 μm step resolution. The 3 × 3 bacteria superarray was stitched together into a hydrogel microstructure ∼66 μm on edge. Loading the sample into the microfluidic, trapping and forming the heterogeneous superarray, photopolymerization, and flushing the microfluidic channel, all took place in under 20 min.

Photopolymerization. To facilitate time-lapse analysis, the bacteria were encapsulated in hydrogel.[11] Hydrogel prepolymer solution consisted of 3.4 kD poly(ethylene glycol) diacrylate (PEGDA, Laysan Bio) at 8% (w/v) (hydrogel monomer); M9 (0.2% glycerol); and a photoinitiator, 2-hydroxy-[4-(hydroxyethoxy)]-2-methyl-1-propanone (Irgacure 2959) at 0.5% (w/v). The bacteria were centrifuged at 2400 rcf for 2.5 min; the supernatant was then aspirated, and the bacterial pellet was resuspended in the prepolymer solution. Cell suspensions were then loaded into 1-mL syringes and injected into microfluidic devices. The prepolymer solution was photopolymerized with 1-s-long exposures using a metal halide light source (X-CITE 120Q, Lumen Dynamics) and a 370 ± 25 nm bandpass UV filter (Semrock). A square mask (∼5.0 mm × 5.0 mm) placed in front of the UV source, was used to control the shape and size of the hydrogel spot. The light generated by the lamp was focused to yield 75 mW/cm^2 at the desired area for photopolymerization.

Fluorescence Imaging. After photopolymerization and flushing the array with M9, we stimulated the arrays by flowing a specific concentrations of AHL (*N*-β-ketocaproyl)-L-homoserine lactone, Sigma) or IPTG (Sigma) and monitored the

resulting fluorescence. Simulations and measurements indicate that the concentration of AHL is uniform throughout the array within about 90 s with a 100 μL/min flush as indicated by the contour plots exhibited in Supplementary Figure S3b,c; the concentration varies by <1% across the superarray.

Fluorescence data was collected using a Leica TCS SP5 II (Leica Microsystems) confocal microscope with enhanced, hybrid *GaAsP* (HyD) detectors for improved sensitivity to fluorescence. All confocal images were acquired using a 100× 1.44NA oil immersion objective (Leica) with an argon laser excitation (488 nm) at 500 nW using a 147.5 μm pinhole (1 Airy unit). Correspondingly, each voxel has a width and height of 178.4 nm and a depth of 377.7 nm for a total volume of 12,030,891 nm^3 or $V_c = 12.0 \times 10^{-18}$ L = 12 aL. Since we used an 8 kHz resonant scanner (with 8 line accumulations), each voxel was exposed for 125 ns at a repetition rate of 8 × 125 ns = 1 μs. The short exposure time and sensitivity of the HyD used for fluorescence detection preclude photobleaching.

Fluorescent z-stacks (along the optic axis) were recorded every 10 min. Around each bacterium, a 5 μm square shaped region-of-interest (ROI) was defined, and the mean intensity in each time-lapse maximum projection image was extracted, yielding time-intensity plots, so-called kymographs. Before the similarity between cellular fluorescence is calculated, the fluorescent signals are conditioned by subtracting the minimum and normalizing the maximum intensity. The logarithmic derivative of the fluorescence was used to improve sensitivity to weak signals.

Laser Flow Cytometry. The threshold AHL concentration for induction in the transformed bacteria was determined by measuring the fluorescence of single bacteria taken from a log-phase culture. First the transformed bacteria were grown from culture in M9-glycerol as described above. Each culture was grown to an OD_{600} of 0.2−0.3 and then induced for 2 h with AHL. The final OD_{600} was 0.4−0.5. Fluorescence data was collected using a FC-500 Beckman-Coulter flow cytometer at a low flow rate, exciting the GFP with a 488 nm argon laser and detecting fluorescence using a (FL-1) 515−545 nm emission filter.

For each concentration of AHL, a fluorescent measurement of gene expression was obtained from one culture. Five measurements were made for each culture: ∼90,000 cells induced at four different AHL concentrations with ∼90,000 uninduced cells used as a control. By gating the forward scatter and side scatter channels, we controlled for cellular size and accounted for morphological variability, providing a better basis for comparison. The threshold concentration for bistability is defined as the AHL concentration for which a bimodal distribution is observed. This is less than the threshold at which expression is 50% of maximum.

Stochastic Simulation of the Dynamic Response of Bacteria to an Inductant. A stochastic model based on mass action equations was developed in order to describe the genetic processes leading to the production of LuxR and GFP in each cell. Schematics of the models are shown in Figures 1b and 5b. The rate equations and parameters for this model that are reproduced in the Supporting Information, and are based on the deterministic equations described elsewhere.[27,28]

Briefly, the inductant IPTG (denoted as I), which can freely diffuse into and out of the cell through the membrane, binds to the lacI repressor that is produced constitutively, which promotes production of LuxI-LVA (U) and GFP-LVA ($G_{l,0}$). LuxI-LVA produces AHL (A) that diffuses out through the cell membrane. Likewise, the constitutive production of LuxR (R) and its degradation, which occurs only by dilution through cell proliferation, were modeled as a first-order kinetic reaction. The AHL binds with R to form P in a second-order kinetic reaction. The product P then dimerizes to form P_2 in another second-order reaction. The dimer P_2 then binds to the operator in the *lux* control region (O_R) and initiates transcription of mRNA for GFP-LVA and LuxR (M_G and M_R, respectively), which is subsequently translated into GFP-LVA(G_0) or R.

The production of R, P, P_2, M_G, M_R, $G_{l,0}$, and G_0 were all modeled by the reactions, and reaction rates are given in the Supporting Information and Supplementary Tables S1 and S2. These rates were inferred, starting with the values compiled from the literature,[27,28] and then varied within a range allowed by experimental error to fit the data including the laser cytometry data, mRNA assays, and fluorescence. The model allows us to track the dynamics of each species in response to variations in the external AHL concentration. The number of species in each cell are calculated from macroscopic quantities by taking into account the estimated volume of the cell: 1 molecule per cell corresponds to approximately $1/(V{\cdot}N_A)$ = 1.7 nM, where N_A is Avogadro's number.

LuxR and GFP production places demands on the cell's resources, e.g., free ribosomes, limiting the resources available for basic metabolism. When MazF is induced, the cell's metabolism slows and the production of most protein (including GFP-LVA and LuxR to a lesser extent) is disrupted. To capture this effect in the model, we modified the rates of LuxR basal production, k_0, and mRNA translation, k_{sG} and k_{sR}, by introducing a dimensionless resource multiplication factor X, (i.e., $k' = Xk$). The value of X was estimated by fitting experimental data to the metabolism sensitive model. We found that X was in the range between 0.15 and 0.3.

Assuming that the system is in thermal equilibrium, the state vector containing the number of molecules of each species is $\chi = \{A_{ex}, A, R, P, P_2, O_R, P_2O_R, M_G, M_R, G_0, G_F\}$. At $t = 0$, $\chi = \{A_{ex}, 0, R_0, 0, 0, O_R, 0, 0, 0, 0, 0\}$, where the initial amount of LuxR in the system is a normally distributed random number R_0 (50 ± 10). The initial number of DNA plasmids (O_R) depends on the copy number in the cell: it is assumed that O_R = 10 for low to medium-copy plasmids and O_R = 40 for high-copy plasmids. For each simulation, external AHL (A_{ex}) is treated as a boundary condition and is not varied by the simulation but depends on the flow condition imposed on the cells in the experiment. The dynamics of the state vector χ is simulated using Gillespie's algorithm[30,48] in MATLAB (The MathWorks, ver.2012a, Natick, MA). Since stochastic simulations rely on an element of probability, we used multiple stochastic runs to account for fluctuations in the behavior of a model. Sensitivity analysis of the model was performed using deterministic solutions to the rate equations.[34]

■ ASSOCIATED CONTENT

Supporting Information

Additional figures and discussion as described in the text. This material is available free of charge via the Internet at http://pubs.acs.org.

■ AUTHOR INFORMATION

Corresponding Author

*E-mail: gtimp@nd.edu.

Author Contributions

†These authors contributed equally to this work.

Notes

The authors declare no competing financial interest.

■ ACKNOWLEDGMENTS

We gratefully acknowledge support from NSF CCF-1129098. We are also grateful to Prof. R. Weiss for the donation of the 203 *lux* plasmid and to Dr. U. Mirsaidov for frequent conversations.

■ REFERENCES

(1) Davey, M. E., and O'Toole, G. A. (2000) Microbial biofilms: From Ecology to Molecular Genetics. *Microbiol. Mol. Biol. Rev. 64* (4), 847−867.
(2) Nobile, C. J., and Mitchell, A. P. (2007) Microbial biofilms: e pluribus unum. *Curr. Biol. 17*, R349−R353.
(3) Davies, D. G., Parsek, M. R., Pearson, J. P., Iglewski, B. H., Costerton, J. W., and Greenberg, E. P. (1998) The involvement of cell-to-cell signals in the development of a bacterial biofilm. *Science 280*, 295−298.
(4) Lewis, K. (2001) Riddle of biofilm resistance. *Antimicrob. Agents Chemother. 45*, 999−1007.
(5) Abraham, W.-R. (2006) Controlling biofilms of Gram-positive pathogenic bacteria. *Curr. Med. Chem. 13*, 1509−1524.
(6) Fuqua, C., Parsek, M. R., and Greenberg, E. P. (2001) Regulation of gene expression by cell-to-cell communication: acyl-homoserine lactone quorum sensing. *Annu. Rev. Genet. 35*, 439−468.
(7) Hentzer, M., Givskov, M., and Eberl, L. (2004) Quorum sensing in biofilms: gossip in slime city, in *Microbial Biofilms* (Ghannoum, M., and O'Toole, G. A., Eds.) pp 118−140, American Society for Microbiology, Washington, DC.
(8) Pappas, K. M., Weingart, C. L., and Winans, S. C. (2004) Chemical communication in proteobacteria: biochemical and structural studies of signal synthases and receptors required for intercellular signalling. *Mol. Microbiol. 53*, 755−769.
(9) Shirtliff, M. E., Mader, J. T., and Camper, A. K. (2002) Molecular interactions in biofilms. *Chem. Biol. 9*, 859−871.
(10) De Kievit, T. R., and Iglewski, B. H. (2000) Bacterial quorum sensing in pathogenic relationships. *Infect. Immun. 68*, 4839−4849.
(11) Timp, W., Mirsaidov, U., Matsudaira, P., and Timp, G. (2009) Jamming prokaryotic cell-to-cell communications in a model biofilm. *Lab Chip 9*, 925−934.
(12) Redfield, R. (2002) Is quorum sensing a side effect of diffusion sensing? *Trends Microbiol. 10*, 365−370.
(13) Hense, B. A., Kuttler, C., Müller, J., Rothballer, M., Hartmann, A., and Kreft, J.-U. (2007) Does efficiency sensing unify diffusion and quorum sensing? *Nat. Rev. Microbiol. 5*, 230−239.
(14) Horswill, A. R., Stoodley, P., Stewart, P. S., and Parsek, M. R. (2007) The effect of the chemical, biological, and physical environment on quorum sensing in structured microbial communities. *Anal. Bioanal. Chem. 387*, 371−380.
(15) Pedraza, J. M., and van Oudenaarden, A. (2005) Noise propagation in gene networks. *Science 307*, 1965−1969.
(16) Raser, J. M., and O'Shea, E. K. (2005) Noise in gene expression: Origins, consequences, and control. *Science 309*, 2010−2013.
(17) Samoilov, M. S., Price, G., and Arkin, A. P. (2006) From fluctuations to phenotypes: The physiology of noise. *Sci. STKE*, re17.
(18) Thattai, M., and van Oudenaarden, A. (2004) Stochastic gene expression in fluctuating environments. *Genetics 167*, 523−530.
(19) Kurz, V., Nelson, E., Perry, N., Timp, W., and Timp, G. (2013) Epigenetic memory emerging from integrated transcription bursts. *Biophys. J 105*, 1526−1532.
(20) Williams, J. W., Cui, X., Levchenko, A., and Stevens, A. M. (2008) Robust and sensitive control of a quorum-sensing circuit by two interlocked feedback loops. *Mol. Syst. Biol. 4*, 234.
(21) Andersen, J. B., Sternberg, C., Poulsen, L. K., Bjørn, S. P., Givskov, M., and Molin, S. (1998) New unstable variants of green fluorescent protein for studies of transient gene expression in bacteria. *Appl. Environ. Microbiol. 64*, 2240−2246.
(22) Mirsaidov, U., Scrimgeour, J., Timp, W., Beck, K., Mir, M., Matsudaira, P., and Timp, G. (2008) Live cell lithography: Using optical tweezers to create synthetic tissue. *Lab Chip 8*, 2174−2181.
(23) Blake, W. J., Balázsi, G., Kohanski, M. A., Isaacs, F. J., Murphy, K. F., Kuang, Y., Cantor, C. R., Walt, D. R., and Collins, J. J. (2006) Phenotypic consequences of promoter-mediated transcriptional noise. *Mol. Cell 24*, 853−865.
(24) Ozbudak, E. M., Thattai, M., Kurtser, I., Grossman, A. D., and van Oudenaarden, A. (2002) Regulation of noise in the expression of a single gene. *Nat. Genet. 31*, 69−73.
(25) McAdams, H. H., and Arkin, A. (1997) Stochastic mechanisms in gene expression. *Proc. Natl. Acad. Sci. U.S.A. 94*, 814−819.
(26) Brenner, K., Karig, D. K., Weiss, R., and Arnold, F. H. (2007) Engineered bidirectional communication mediates a consensus in a microbial biofilm consortium. *Proc. Natl. Acad. Sci. U.S.A. 104*, 17300−17304.
(27) Goryachev, A. B., Toh, D. J., and Lee, T. (2006) Systems analysis of a quorum sensing network: Design constraints imposed by the functional requirements, network topology and kinetic constants. *Biosystems 83*, 178−187.
(28) Stamatakis, M., and Mantzaris, N. V. (2009) Comparison of deterministic and stochastic models of the lac operon genetic network. *Biophys. J. 96*, 887−906.
(29) Suzuki, M., Mao, L., and Inouye, M. (2007) Single protein production (SPP) system in Escherichia coli. *Nat. Protoc. 2*, 1802−1810.
(30) Gillespie, D. T. (1977) Exact stochastic simulation of coupled chemical reactions. *J. Phys. Chem. 81*, 2340−2361.
(31) Wu, Y., Joseph, S., and Aluru, N. R. (2009) Effect of cross-linking on the diffusion of water, ions, and small molecules in hydrogels. *J. Phys. Chem. B 113*, 3512−3520.
(32) Culbertson, M. J., Williams, J. T. B., Cheng, W.W. L., Stults, D. E., Wiebracht, E. R., Kasianowicz, J. J., and Burden, D. L. (2007) Numerical fluorescence correlation spectroscopy for the analysis of molecular dynamics under nonstandard conditions. *Anal. Chem. 79*, 4031−4039. Zhang, L., Dammann, K., Baeb, K. C., and Granick, S. (2007) Ligand−receptor binding on nanoparticle-stabilized liposome surfaces. *Soft Matter 3*, 551−553.
(33) Rosenblum, M. G., Pikovsky, A. S., and Kurths, J. (1997) From phase to lag synchronization in coupled chaotic oscillators. *Phys. Rev. Lett. 78*, 4193−4196.
(34) Ingalls, B. P., and Sauro, H. M. (2003) Sensitivity analysis of stoichiometric networks: an extension of metabolic control analysis to non-steady state trajectories. *J. Theor. Biol. 222*, 23−36.
(35) Dunaway, M., Olson, J. S., Rosenberg, J. M., Kallai, O. B., Dickerson, R. E., and Matthews, K. S. (1980) Kinetic studies of inducer binding to lac repressor-operator complex. *J. Biol. Chem. 255*, 10115−10119.
(36) Gilbert, W., and Müller-Hill, B. (1966) Isolation of the lac repressor. *Proc. Natl. Acad. Sci. U.S.A. 56*, 1891−1898.
(37) O'Gorman, R. B., Rosenberg, J. M., Kallai, O. B., Dickerson, R. E., Itakura, K., Riggs, A. D., and Matthews, K. S. (1980) Equilibrium binding of inducer to lac repressor operator DNA complex. *J. Biol. Chem. 255*, 10107−10114.
(38) Strathmann, M., Greibe, T., and Flemming, H.-C. (2000) Artificial biofilm model—a useful tool for biofilm research. *Appl. Microbiol. Biotechnol. 54*, 231−237.
(39) Akselrod, G., Timp, W., Timp, K., Timp, R., and Timp, G. (2006) Laser-guided assembly of living cell microarrays. *Biophys. J. 91*, 3456−3474.
(40) Perry, N., Nelson, E., Kurz, V., Sarveswaran, K., Kyrouac, D., Mirsaidov, U., and Timp, G. (2013) Wiring a biological integrated circuit, *Lab Chip*, submitted for publication.
(41) Novick, A., and Weiner, M. (1957) Enzyme induction as an all-or-none phenomenon. *Proc. Natl. Acad. Sci. U.S.A. 43*, 553−566.

(42) Isaacs, F. J., Hasty, J., Cantorand, C. R., and Collins, J. J. (2003) Prediction and measurement of an autoregulatory genetic module. *Proc. Natl. Acad. Sci. U.S.A. 100*, 7714−7719.
(43) McMillen, D., Kopell, N., Hasty, J., and Collins, J. J. (2002) Synchronizing genetic relaxation oscillators by intercell signaling. *Proc. Natl. Acad. Sci. U.S.A. 99*, 679−684.
(44) Danino, T., Mondragon-Palomino, O., Tsimring, L., and Hasty, J. (2010) A synchronized quorum of genetic clocks. *Nature 463*, 326−330.
(45) Rao, C. V., Wolf, D. M., and Arkin, A. P. (2002) Control, exploitation and tolerance of intracellular noise. *Nature 420*, 231−237.
(46) Williams, P., Winzer, K., Chan, W. C., and Cámara, M. (2007) Look who's talking: communication and quorum sensing in the bacterial world. *Philos. Trans. R. Soc., B 362*, 1119−1134.
(47) Reeve, J. N. (1992) Molecular biology of methanogens. *Annu. Rev. Microbiol. 46*, 165−191.
(48) Hindmarsh, A. C., Brown, P. N., Grant, K. E., Lee, S. L., Serban, R., Shumaker, D. E., and Woodward, C. S. (2005) SUNDIALS: Suite of nonlinear and differential/algebraic equation solvers. *ACM Trans. Math. Software 31*, 363−396.